

# Spectral representation analysis of dielectric screening in solids and molecules

Amandeep Kaur,<sup>1,\*</sup> Erik R. Ylvisaker,<sup>1</sup> Deyu Lu,<sup>2</sup> Tuan Anh Pham,<sup>3</sup> Giulia Galli,<sup>1,3</sup> and Warren E. Pickett<sup>1</sup>

<sup>1</sup>*Department of Physics, University of California, Davis, Davis, California 95616, USA*

<sup>2</sup>*Center for Functional Nanomaterials, Brookhaven National Laboratory, Upton, New York 11973, USA*

<sup>3</sup>*Department of Chemistry, University of California, Davis, Davis, California 95616, USA*

(Received 24 October 2012; revised manuscript received 20 March 2013; published 24 April 2013)

We propose a new approach to identifying and rationalizing the contribution of core electron polarization to dielectric screening, based on *ab initio* calculations of the dielectric matrix in its eigenpotential basis. We also present calculations of phonon frequencies, dielectric constants, and quasiparticle energies of several systems, and we discuss the quantitative effect of including core polarization. Our findings illustrate efficient ways of approximating the spectral decomposition of dielectric matrices used, e.g., in many-body perturbation theory and dielectric constant calculations, with substantial computational gains for large systems composed of heavy atoms.

DOI: [10.1103/PhysRevB.87.155144](https://doi.org/10.1103/PhysRevB.87.155144)

PACS number(s): 77.22.Ej, 71.15.Mb, 71.15.Qe, 77.22.Ch

## I. INTRODUCTION

Understanding the microscopic origin of dielectric screening<sup>1–4</sup> is central to rationalizing vibrational and excited-state properties of condensed and molecular systems and, ultimately, their chemical bonding. Many calculations of solids, liquids, and molecules appearing in the last several decades are based on a partitioning of the interacting electrons into core and valence: the former are assumed to be in the same configuration as in the constituent atoms, and the latter participate in the dielectric screening in the condensed and molecular phases. The extent to which core polarization affects electronic screening and thus physical properties such as phonon frequencies, dielectric constants, and electronic excitation spectra is seldom analyzed. Few theoretical studies have addressed core polarization effects on quasiparticle (QP) energies,<sup>5–8</sup> which have been found to be more important, both qualitatively and quantitatively, than previously thought. It is therefore of interest to understand and analyze the origin of such effects and establish modeling frameworks to take them into account in a consistent and accurate manner.

Shirley *et al.*<sup>5,6</sup> pointed out the importance of including  $3d$  electrons in the valence partition of certain elemental semiconductors, in order to obtain accurate values of their band gaps within many-body perturbation theory at the non-self-consistent *GW*<sup>9,10</sup> level, and they proposed using pseudopotentials (PPs) that explicitly account for core polarization. Similar results were reported in Refs. 11–13 for CdS. However, Ku *et al.*<sup>14</sup> later observed that, within the *self-consistent GW*,<sup>15</sup> the inclusion of polarization from  $3d$  electrons does not affect, e.g., the computed band gap of Ge.

Recently Gómez-Abal *et al.*<sup>7</sup> and Li *et al.*<sup>16</sup> computed the electronic properties of several crystalline solids and showed that in *GW* calculations there are substantial differences in the matrix elements of the exchange part of the self-energy ( $\Sigma_x$ ) and exchange-correlation potential ( $V_{xc}$ ), depending on the choice of the core-valence partition. These findings are consistent with earlier results of Marini *et al.*,<sup>8</sup> who showed that exchange-correlation contributions to the self-energy arising from the  $3s$  and  $3p$  semicore levels of Cu should be

taken into account to obtain a QP band structure in agreement with experiments. Other studies<sup>7,16</sup> also noted that for systems without  $d$  electrons, the most substantial differences in band gaps, between all-electron and PP calculations, arose from the correlation part of the self-energy ( $\Sigma_c$ ), as there is an almost-complete cancellation between the matrix elements of  $\Sigma_x$  and  $V_{xc}$ . Umari *et al.*<sup>17</sup> analyzed the effect of semicore states on the electronic structure of the metal phthalocyanine molecule and noted that Zn  $3s$  and  $3p$  states need to be included in the valence to accurately describe photoemission spectra.

In this paper we propose a new approach for identifying and analyzing the contribution of core electron polarization to dielectric screening, based on the spectral decomposition of the dielectric matrix (DM).<sup>18,19</sup> We present *ab initio* calculations of dielectric band structures (DBSs), inverse participation ratios (IPR), density of states (DOS) of the DM, phonon frequencies, dielectric constants, and QP gaps of several systems, and we discuss the quantitative effect of including core polarization.

The rest of the paper is organized as follows. We describe the method for computing the dielectric spectra for solids and molecules in Sec. II. In Sec. III we present our results for the DBS and IPR analysis of solids, followed by the discussion of the DOS and IPR of molecules in Sec. IV. Section V discusses the relationship among the DBS, phonons, and nonlinear core corrections (NLCCs), which is followed by results of core-polarization effects on QP energies (Sec. VI). We summarize our findings in Sec. VII.

## II. THEORETICAL BACKGROUND

In the linear regime, the static dielectric screening is expressed by the function  $\epsilon(\mathbf{r}, \mathbf{r}')$ , which relates the external potential applied to a system of electrons,  $V_{\text{ext}}$ , and the resulting screened potential:

$$V_{\text{scr}}(\mathbf{r}) = \int \epsilon(\mathbf{r}, \mathbf{r}')^{-1} V_{\text{ext}}(\mathbf{r}') d\mathbf{r}'. \quad (1)$$

We refer to  $\epsilon$  as the DM and we restrict our analysis to DMs obtained within the random phase approximation (RPA),<sup>20,21</sup> although the formalism presented here is general and may

be applied to dielectric screening obtained at higher levels of theory. Within the RPA, the DM is defined as

$$\epsilon = 1 - v_c \cdot \chi^0, \quad (2)$$

where  $v_c$  is the Coulomb potential and  $\chi^0$  is the noninteracting density response function, which is related to the interacting one via the equation

$$\chi = (1 - \chi^0 \cdot v_c)^{-1} \cdot \chi^0, \quad (3)$$

where in Eqs. (2) and (3) integrals are implicit.

Within a plane-wave representation where wave functions are expressed as linear combinations of plane waves [ $\exp(i\mathbf{G} \cdot \mathbf{r})$ ;  $\mathbf{G}$  is a reciprocal wave vector], for doubly filled shells,  $\epsilon$  is defined as in Eq. (4), where  $\mathbf{k}$  and  $\mathbf{q}$  denote wave vectors, and  $\epsilon_{v,\mathbf{k}}$ ,  $\epsilon_{c,\mathbf{k}}$  are energies of the valence ( $v$ ) and conduction ( $c$ ) single-particle states, respectively. In the case of molecules, one only considers  $\mathbf{k} = 0$  and  $\mathbf{q} \rightarrow 0$ , and valence and conduction states correspond to the occupied and empty (or virtual) states, respectively:

$$\begin{aligned} \epsilon_{\mathbf{G},\mathbf{G}'}(\mathbf{q}) &= \delta_{\mathbf{G},\mathbf{G}'} - \frac{4\pi e^2}{|\mathbf{q} + \mathbf{G}|^2} \frac{4}{N_{\mathbf{k}}\Omega} \sum_{c\nu\mathbf{k}} \\ &\times \frac{\langle v, \mathbf{k} | e^{-i(\mathbf{q} + \mathbf{G}) \cdot \mathbf{r}} | c, \mathbf{k} + \mathbf{q} \rangle \langle c, \mathbf{k} + \mathbf{q} | e^{i(\mathbf{q} + \mathbf{G}') \cdot \mathbf{r}'} | v, \mathbf{k} \rangle}{\epsilon_{v,\mathbf{k}} - \epsilon_{c,\mathbf{k} + \mathbf{q}}}. \end{aligned} \quad (4)$$

It is both formally and computationally convenient to introduce the symmetric form of the DM:

$$\tilde{\epsilon}_{\mathbf{G},\mathbf{G}'}(\mathbf{q}) = \frac{|\mathbf{q} + \mathbf{G}|}{|\mathbf{q} + \mathbf{G}'|} \epsilon_{\mathbf{G},\mathbf{G}'}(\mathbf{q}). \quad (5)$$

The symmetrized  $\tilde{\epsilon}^{-1}$  can be diagonalized to obtain the dielectric eigenvalue spectrum  $\lambda_m^{-1}(\mathbf{q})$  and eigenpotentials  $\zeta_m(\mathbf{q})$ :

$$\sum_{\mathbf{G}'} \tilde{\epsilon}_{\mathbf{G},\mathbf{G}'}^{-1}(\mathbf{q}) \langle \mathbf{G}' | \zeta_m(\mathbf{q}) \rangle = \lambda_m^{-1}(\mathbf{q}) \langle \mathbf{G} | \zeta_m(\mathbf{q}) \rangle. \quad (6)$$

The DBS<sup>1-3</sup> is defined as  $\lambda_m^{-1}(\mathbf{q})$  vs  $\mathbf{q}$ , in a manner analogous to the eigenvalues of the Hamiltonian of a periodic solid as a function of the wave vector, which defines an electronic band structure.

For each of the solid and molecular systems investigated in the next sections, we define two different partitions of the core and valence electrons in our electronic structure and density functional perturbation theory calculations. We specify core, semicore, and valence electrons. The core electrons are the same in both partitions. In one partition we include semicore electrons in the valence, i.e., we consider them to participate in the chemical bonding. We call this partition a semicore (SC) one and the corresponding DM  $\tilde{\epsilon}^{\text{SC}}$ :

$$(\tilde{\epsilon}^{\text{SC}})^{-1} = \sum_i (\lambda_i^{\text{SC}})^{-1} |\zeta_i^{\text{SC}}\rangle \langle \zeta_i^{\text{SC}}|. \quad (7)$$

The other partition includes semicore electrons in the core; i.e., we consider the latter frozen and not participating in the chemical bonding. We call this a valence electron (VE) partition and the corresponding DM  $\tilde{\epsilon}^{\text{VE}}$ :

$$(\tilde{\epsilon}^{\text{VE}})^{-1} = \sum_i (\lambda_i^{\text{VE}})^{-1} |\zeta_i^{\text{VE}}\rangle \langle \zeta_i^{\text{VE}}|. \quad (8)$$

To characterize the localization properties of the eigenvectors of the DM, or eigenpotentials, we define the IPR as

$$\text{IPR}_m = \frac{\frac{1}{N} \sum_{i=1}^N |\zeta_m(\mathbf{r}_i)|^4}{\left[\frac{1}{N} \sum_{i=1}^N |\zeta_m(\mathbf{r}_i)|^2\right]^2}, \quad (9)$$

where  $N$  is the number of points in the real-space grid used to represent the eigenpotential  $\zeta_m$ . An IPR value of 1 indicates that the mode is completely delocalized and the value increases from 1 with the localization of the eigenpotential.

To analyze the distribution of the dielectric eigenvalues, we calculated the DOSs of the DM. A useful measure of the difference between the eigenpotentials of  $(\tilde{\epsilon}^{\text{SC}})^{-1}$  and those of  $(\tilde{\epsilon}^{\text{VE}})^{-1}$  is given by the projection ( $F_m$ ) of the  $m$ th eigenpotential of the  $(\tilde{\epsilon}^{\text{SC}})^{-1}$ ,  $(\zeta_m^{\text{SC}})$ , on the VE potential eigenspace:

$$F_m = \langle \zeta_m^{\text{SC}} | I_v | \zeta_m^{\text{SC}} \rangle, \quad I_v = \sum_j |\zeta_j^{\text{VE}}\rangle \langle \zeta_j^{\text{VE}}|. \quad (10)$$

We define the DOS as

$$g_w(\lambda^{-1}) = (1 - \lambda^{-1}) \sum_m w_m \delta(\lambda^{-1} - \lambda_m^{-1}). \quad (11)$$

The prefactor is included for presentation purposes, to temper the large values of the DOSs as the eigenvalues of  $\tilde{\epsilon}^{-1} \rightarrow 1$ . Here  $w_m = 1$  corresponds to the unweighted DOS and  $w_m = F_m$  corresponds to weighting of the DOS according to the projection of the eigenmodes of  $(\tilde{\epsilon}^{\text{SC}})^{-1}$  onto the VE-only subspace.

The eigenvalues and eigenvectors of the DM were computed using an iterative<sup>18,19,22,23</sup> procedure built into codes that are postprocessing modules of Quantum Espresso.<sup>24</sup> We studied DBS and phonons of alkali hydride crystals, dielectric spectra, and QP gaps of alkali halide molecules, alkali dimers, and alkaline earth oxides. We considered experimental structures (except where noted) for all systems. We used the local density approximation (LDA) and norm-conserving semirelativistic PPs in the separable form proposed by Hartwigsen-Goedecker-Hutter.<sup>25</sup>

### III. DIELECTRIC BAND STRUCTURE AND INVERSE PARTICIPATION RATIO ANALYSIS: CRYSTALLINE NaH

Figure 1 shows the DBS of the simple ionic insulator NaH computed with two different core-valence partitions. The VE partition includes only the  $3s^1$  electron of Na; the SC partition includes the  $(2s^2 2p^6)3s^1$  electrons. The (colored) circles in Figs. 1(a) and 1(b) show the magnitude of the projections  $\langle \zeta_m^{\text{SC}}(\mathbf{q}_0) | \zeta_j^{\text{VE}}(\mathbf{q}) \rangle$  and  $\langle \zeta_m^{\text{SC}}(\mathbf{q}_0) | \zeta_j^{\text{SC}}(\mathbf{q}) \rangle$  of the eigenpotentials of  $(\tilde{\epsilon}^{\text{SC}})^{-1}$ ,  $|\zeta_m^{\text{SC}}(\mathbf{q}_0)\rangle$  at a  $\mathbf{q}_0$  point near  $\mathbf{q} = 0$  onto the eigenpotentials of  $(\tilde{\epsilon}^{\text{VE}})^{-1}$  and  $(\tilde{\epsilon}^{\text{SC}})^{-1}$ , respectively, at all the  $\mathbf{q}$  points along the [100] direction. There are qualitative differences between the VE and the SC DBSs, despite the rather strong binding of the  $2s$  ( $-50$  eV) and  $2p$  ( $-22$  eV) levels. From Eq. (4), one might expect the large energy denominator to lead to fully negligible contributions of the core states to the eigenvalues of  $\tilde{\epsilon}^{-1}$ . However, we observed the appearance of bands with  $\lambda_m^{-1}$  well below unity (which corresponds to additional screening) when using the SC

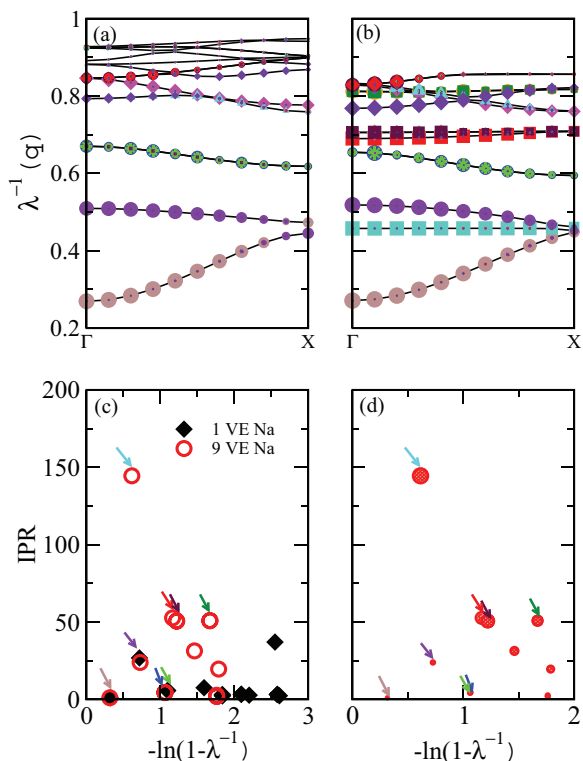


FIG. 1. (Color online) Lowest 15 bands of the dielectric band structure (DBS) for fcc crystal NaH obtained by using core valence partitions with (a) one valence electron (VE) and (b) nine VEs (SC) for Na (see text). The (colored) circles in (a) and (b) show the magnitude of the projections  $\langle \zeta_m^{\text{SC}}(\mathbf{q}_0) | \zeta_j^{\text{VE}}(\mathbf{q}) \rangle$  and  $\langle \zeta_m^{\text{SC}}(\mathbf{q}_0) | \zeta_j^{\text{SC}}(\mathbf{q}) \rangle$  of the eigenpotentials of  $(\tilde{\epsilon}^{\text{SC}})^{-1}$ ,  $|\zeta_m^{\text{SC}}(\mathbf{q}_0)\rangle$  at a  $\mathbf{q}_0$  point near  $\mathbf{q} = 0$  onto the eigenpotentials of  $(\tilde{\epsilon}^{\text{VE}})^{-1}$  and  $(\tilde{\epsilon}^{\text{SC}})^{-1}$ , respectively. (c) Inverse participation ratio (IPR) of the DM eigenpotentials of the SC and VE partitions at the  $\Gamma$  point. (d) IPR; the circle size is the projection  $(1 - F_m)$  as defined in Eq. (10) for the SC eigenpotentials at the  $\Gamma$  point. The color code used for the arrows is the same as that used for the eigenpotentials in (a) and (b).

partition. For example, a band appears with  $\lambda_m^{-1} = 0.45$  at  $\Gamma$ ; two additional bands appear around 0.7. In addition, there are other bands closer to unity, and some bands present in the spectrum obtained with the VE partition are shifted, as the SC character of the eigenpotentials is mixed with the VE character.

Figure 1(c) shows the IPR of the eigenmodes obtained with the SC and VE partitions at the  $\Gamma$  point. The color code used for the arrows in Figs. 1(c) and 1(d) is the same as the one adopted for the eigenpotentials in Figs. 1(a) and 1(b). Note the log scale on the abscissa, chosen to better distinguish the eigenvalues near 1. The eigenmodes obtained with the VE partition have relatively low IPR values compared to the ones computed for the SC partition. However, the first SC and VE eigenmodes at  $\Gamma$  are completely delocalized ( $\text{IPR} \approx 1$ ). In Fig. 1(c), the second eigenmode, which has a predominantly SC character (it is not present in the calculation with the VE partition), has a relatively high value of IPR.

To classify the SC eigenmodes further, Fig. 1(d) shows the VE fraction of the SC eigenmodes at the  $\Gamma$  point: each SC eigenpotential is projected onto the VE potential eigenspace

[Eq. (10)], and we represent  $(1 - F_m)$  as a circle for each eigenstate. The VE fraction  $F_m$  depicts the character of the eigenmodes obtained using the SC partition: the smaller  $F_m$  (larger  $1 - F_m$ ) (and larger circle size), the more predominant is the SC character; the larger  $F_m$  (smaller  $1 - F_m$ ) (and smaller circle size), the more predominant is the VE character.

#### IV. DENSITY OF STATES OF THE DIELECTRIC MATRIX AND PARTICIPATION RATIO: MOLECULES

We analyzed the dielectric spectra of several molecules representative of both ionic and covalent bonding including alkali dimers ( $\text{Rb}_2$ ,  $\text{K}_2$ ,  $\text{Na}_2$ ,  $\text{Li}_2$ ), alkali halides ( $\text{KI}$ ,  $\text{KCl}$ ,  $\text{NaCl}$ ), and alkaline earth oxides ( $\text{CaO}$ ,  $\text{SrO}$ ) by varying the core-valence partition of the cation. Similarly to the case of the NaH crystal presented earlier, for Li, K, Rb, Ca, and Sr we considered  $(1s^2)2s^1$ ,  $(3s^2, 3p^6)4s^1$ ,  $(4s^2, 4p^6)5s^1$ ,  $(3s^2, 3p^6)4s^2$ , and  $(4s^2, 4p^6)5s^2$  configurations, respectively. We studied the distribution of the dielectric eigenvalues of these molecules by calculating the DOS as defined in Eq. (11).

We consider the dielectric matrices  $(\tilde{\epsilon}^{\text{VE}})^{-1}$  and  $(\tilde{\epsilon}^{\text{SC}})^{-1}$  and we analyze their respective eigenvalues, eigenpotential character, and eigenpotential localization properties. We discuss below three main findings: (i) the inclusion of semicore electrons in the screening of the Coulomb potential has a global

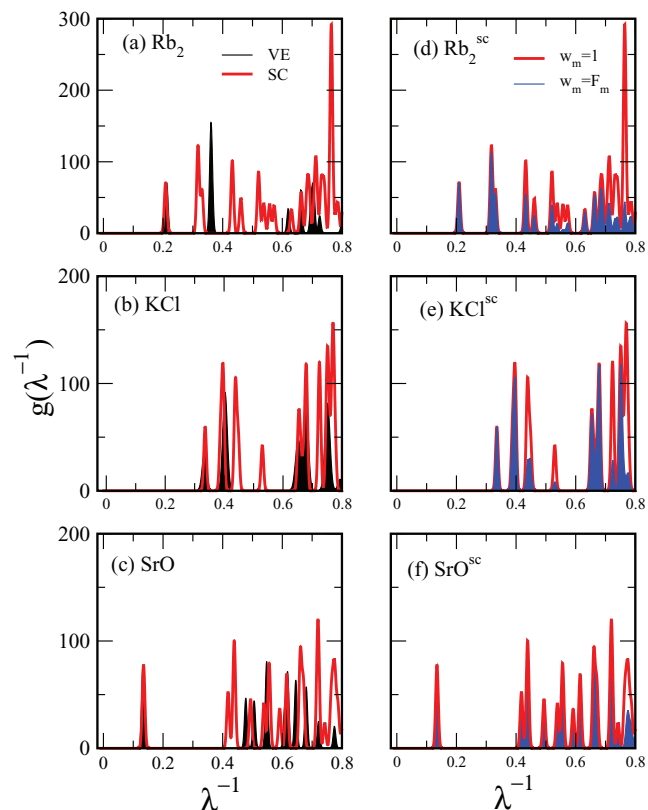


FIG. 2. (Color online) Density of states of the dielectric matrix  $g(\lambda^{-1}) = \sum_m \delta(\lambda^{-1} - \lambda_m^{-1}) \cdot w_m \cdot (1 - \lambda^{-1})$  as a function of the eigenvalue  $\lambda$  for the  $\text{Rb}_2$  dimer,  $\text{KCl}$  molecule, and  $\text{SrO}$  molecule, where the weight  $w_m$  is defined in Eq. (10). (a-c) Density of states of  $(\tilde{\epsilon}^{\text{SC}})^{-1}$  [red; see Eq. (7)] and  $(\tilde{\epsilon}^{\text{VE}})^{-1}$  [black; see Eq. (8)] for  $w_m = 1$ . (d-f) Density of states of  $(\tilde{\epsilon}^{\text{SC}})^{-1}$  for  $w_m = 1$  [red; the same as reported in (a-c)] and  $w_m = F_m$  [blue; see Eq. (10)].

influence on the eigenvalues of  $\tilde{\epsilon}^{-1}$ , i.e., the set of eigenvalues of  $(\tilde{\epsilon}^{\text{SC}})^{-1}$  may not be separated into subsets corresponding to eigenpotentials with a clearly defined SC or VE character; (ii) the character of the eigenpotentials depends on the type of bonding in the system; and (iii) the correlation between the eigenpotentials' character and their localization properties depends again on the bonding properties.

We illustrate finding i in Figs. 2(a), 2(b), and 2(c), which show the DOS of  $(\tilde{\epsilon}^{\text{SC}})^{-1}$  and that of  $(\tilde{\epsilon}^{\text{VE}})^{-1}$  for the  $\text{Rb}_2$ ,  $\text{KCl}$ , and  $\text{SrO}$  molecules, respectively. These molecules are taken to be representative of each class of molecules considered in our study. It is apparent from the figures that a clear separation of eigenvalues into SC-like and VE-like ones is not possible. The distribution of those that may be classified as SC-like and VE-like strongly depends on the type of bonding in the system.

We now turn to discussing the character of eigenpotentials obtained using SC partition, illustrated in Figs. 2(d)–2(f), where we compare the DOS of  $(\tilde{\epsilon}^{\text{SC}})^{-1}$  for two cases:  $w_m = 1$  and  $w_m = F_m$  [see Eq. (11)]. It is seen once more that the character of the eigenpotentials depends on the bonding, e.g., in the case of  $\text{SrO}$  one observes small changes for the two values of  $w_m$ , whereas substantial changes are present in the case of  $\text{Rb}_2$  and  $\text{KCl}$ .

This observation of differences in the eigenpotential character, depending on the type of bonds, is further strengthened by the correlation between character and localization, shown in Fig. 3, where we plot the mode IPR as a function of the eigenvalues for the eigenmodes obtained using SC partition, and we represent the weight  $F_m$  of the eigenmodes by the symbol size. For oxides [Fig. 3(c)], the highest localized modes have a predominantly VE character, as indicated by the small values of  $(1 - F_m) \approx 0$ –0.2. This is consistent with our analysis of the DOS of  $\text{SrO}$ . For the alkali dimers [Fig. 3(a)]

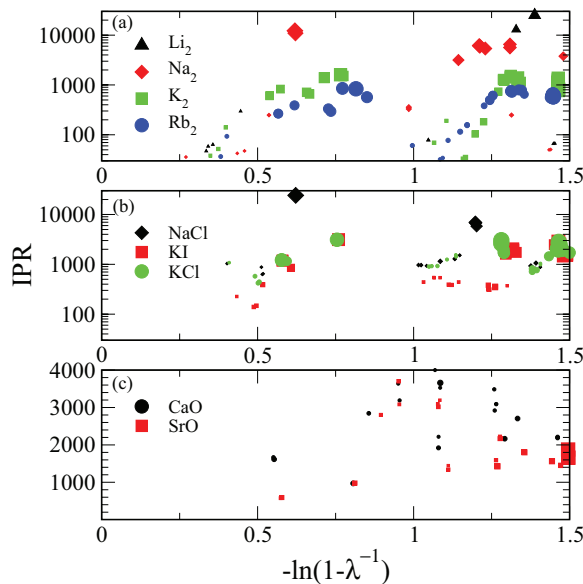


FIG. 3. (Color online) Inverse participation ratio (IPR) as a function of the eigenvalues  $\lambda$  of  $(\tilde{\epsilon}^{\text{SC}})^{-1}$ ; the circle size is the projection  $(1 - F_m)$  [see Eq. (10)] for (a) alkali dimers, (b) alkali halides, and (c) alkaline earth oxides. The log scale on the abscissa is chosen to better distinguish the eigenvalues near 1, where they would become very dense on a linear scale.

and alkali halides [Fig. 3(b)] the most localized eigenmodes have a predominantly SC character, similar to the case of  $\text{NaH}$ . The density of high-IPR modes is more for alkali dimers compared to alkali halides. Highly localized eigenmodes are present in  $\text{Na}_2$  and, more so, in  $\text{K}_2$  and  $\text{Rb}_2$ , indicating substantial screening by semicore electrons, consistent with our findings for phonons in the next section. A point to note here is that the dipole polarizability of the  $\text{Rb}$  atom (319 a.u.) is the highest of all the alkali and alkaline earth atoms considered in this study, followed by  $\text{K}$  (291 a.u.) and  $\text{Sr}$  (186 a.u.).

We conclude, therefore that upon adding semicore electrons to the VE partition, the dielectric response varies both by the type of bonding and by the atomic size of the constituents. More screening channels appear for covalently bonded alkali dimers compared to ionic molecules, with no appreciable change in the screening for alkaline earth oxides. As expected, the contribution of semicore electrons to screening is larger for larger alkali atoms.

## V. DIELECTRIC BAND STRUCTURE AND PHONONS

In this section we present results for phonon frequencies and dielectric constants, obtained using different core-valence partitions. We also compared our findings with results obtained with NLCC,<sup>26,27</sup> often used in the literature to include the contribution of semicore electrons. We show below that results obtained with NLCC and the SC partition differ and we discuss the origin of these differences.

The dynamical matrix of a solid is given by the sum of an unscreened ionic part ( $I$ ) and a screening part ( $E$ ),

$$D_{ss'}^{\alpha\beta}(\mathbf{q}) = (D_{ss'}^{\alpha\beta}(\mathbf{q}))^I + (D_{ss'}^{\alpha\beta}(\mathbf{q}))^E, \quad (12)$$

where  $\alpha$  and  $\beta$  are Cartesian components and  $s$  and  $s'$  label the atoms in the unit cell. The first term  $[D_{ss'}^{\alpha\beta}(\mathbf{q})]^I$  contains the direct Coulomb interaction between the ion cores in the crystal. The term  $[D_{ss'}^{\alpha\beta}(\mathbf{q})]^E$  is given by

$$(D_{ss'}^{\alpha\beta}(\mathbf{q}))^E = \frac{1}{(M_s M_{s'})^{1/2}} \left( C_{ss'}^{\alpha\beta}(\mathbf{q}) - \delta_{ss'} \sum_{s''} C_{ss''}^{\alpha\beta}(0) \right). \quad (13)$$

The force constants  $C$  are defined as

$$\begin{aligned} C_{ss'}^{\alpha\beta}(\mathbf{q}) &= \frac{\Omega}{4\pi e^2} \sum_{\mathbf{G}\mathbf{G}'} (\mathbf{q} + \mathbf{G})_\alpha V_s(\mathbf{q} + \mathbf{G}) \\ &\times e^{i\mathbf{G}\cdot\mathbf{R}_s} |\mathbf{q} + \mathbf{G}|^2 [\epsilon_{\mathbf{G}\mathbf{G}'}^{-1}(\mathbf{q}) - \delta_{\mathbf{G}\mathbf{G}'}] (\mathbf{q} + \mathbf{G}')_\beta \\ &\times V_{s'}'(\mathbf{q} + \mathbf{G}') e^{-i\mathbf{G}'\cdot\mathbf{R}_{s'}}, \end{aligned} \quad (14)$$

where  $M_s$  is the nuclear mass of the  $s$ th atom in the unit cell,  $\Omega$  is the unit cell volume,  $\mathbf{R}_s$  is the position vector of the ion cores, and  $V_s$  is the bare ion PP. Depending on the choice of the core-valence partition in the calculations of  $\epsilon$  in Eq. (14), one expects to obtain different results for phonon frequencies.

The results for nine VEs (corresponding to the SC partition) for solids containing,  $\text{Na}$ ,  $\text{K}$ , and  $\text{Rb}$  at optimized geometries are comparable with the previous phonon calculations,<sup>28,29</sup> with differences, with regard to Refs. 28 and 29, of less than 4% in the phonon frequencies. There are important differences between SC and VE results and they become increasingly important for the heavier alkali hydrides, reflecting strong contributions from semicore states. In the case of  $\text{NaH}$ , for

TABLE I. Zone-center phonon frequencies ( $\text{cm}^{-1}$ ) of the transverse ( $\omega_{\text{TO}}$ ) and longitudinal ( $\omega_{\text{LO}}$ ) optical modes of fcc NaH, KH, and RbH crystal, and electronic ( $\epsilon^\infty$ ) and static dielectric constant ( $\epsilon^0$ ). Two core-level partitions were used for Na, K, and Rb [nine valence electrons (VEs) and one VE], and results are also given for calculation with one VE and a nonlinear core correction (NLCC). Results are presented both for the experimental lattice constant and for the optimized geometry at the LDA level.

	$\omega_{\text{TO}}$	$\omega_{\text{LO}}$	$\epsilon^\infty$	$\epsilon^0$
NaH				
Experimental geometry				
1 VE	330	801	3.27	19.3
9 VEs	432	832	3.35	12.4
1 VE + NLCC	438	837	3.2	11.7
Optimized geometry				
1 VE	540	934	3.31	9.9
9 VEs	561	917	3.36	9.0
1 VE + NLCC	568	925	3.2	8.5
KH				
Experimental geometry				
9 VEs	405	726	2.9	9.3
1 VE + NLCC	376	708	2.5	8.7
Optimized geometry				
9 VEs	519	808	2.9	7.2
1 VE + NLCC	613	876	2.4	4.9
RbH				
Experimental geometry				
9 VEs	371	678	3.0	10.0
1 VE + NLCC	340	663	2.4	9.0
Optimized geometry				
9 VEs	481	759	3.1	7.8
1 VE + NLCC	604	859	2.4	4.9

example, the transverse optical frequencies  $\omega_{\text{TO}}$  and the dielectric constant (Table I) evaluated using one VE for Na differ from SC calculations by 23% and 56%, respectively, when the experimental volume is used. The difference becomes larger for KH and RbH (Table I). This result is not unexpected, since it is known<sup>26,28,30</sup> that, when using PPs to describe materials containing alkali atoms, semicore electronic states must be included in the calculation.

It was previously reported that the use of NLCC,<sup>31,32</sup> which accounts for the rigid shift of the semicore density as the nucleus moves, provides, in many cases, a good description of the phonons. We computed the DBS of LiH (not shown) and NaH using NLCC; the results differed by less than 2% from those obtained by VE calculations. Hence the use of NLCC does not account for the appearance of the additional eigenmodes observed in SC calculations. This correction is different from the full SC treatment, because in the latter the semicore electrons (i) respond self-consistently to changes in the potential not due to nuclear motion and (ii) respond nonrigidly to the nuclear motion. However, NLCC is useful when there is strong spatial overlap of the semicore and valence wave functions, such as in the alkali atoms. As reported in Table I for NaH, NLCC accounts for most of the difference between SC and VE phonon frequencies, although additional differences of a few percent remain (4%–5% in the value of  $\epsilon^0$ ). For the heavier alkali hydrides, the use of NLCC is

progressively less accurate. For RbH, the remaining error is around 10% for  $\epsilon^0$  and reflects the effect of core *polarization* rather than simple rigid displacement of the core charge. We note that the error becomes worse if the volume is optimized including NLCC, instead of considering the experimental volume: the error is more than 37% for  $\epsilon^0$  and 25% for  $\omega_{\text{TO}}$ . Evidently, SC screening becomes more important as the volume decreases.

## VI. CORE POLARIZATION EFFECTS ON QUASIPARTICLE ENERGIES FOR MOLECULES

We carried out *GW* calculations for molecules using the method of Nguyen *et al.*<sup>45</sup> and obtained QP energies ( $E_i^{\text{QP}}$ ):

$$E_i^{\text{QP}} = \epsilon_i + \langle \psi_i | [\Sigma_c(E_i^{\text{QP}}) + \Sigma_x - V_{xc}] | \psi_i \rangle. \quad (15)$$

Here  $\psi_i$  and  $\epsilon_i$  are the eigenvectors and eigenvalues of the Kohn-Sham (KS) Hamiltonian. The correlation contribution to the self-energy is given by

$$\Sigma_c(\omega) = \frac{i}{2\pi} \int G(\mathbf{r}, \mathbf{r}'; \omega + \omega') W^c(\mathbf{r}, \mathbf{r}'; \omega') d\omega', \quad (16)$$

where  $W^c = W - v_c$  and  $W$  is the screened Coulomb potential, given by

$$W = \epsilon^{-1} \cdot v_c = v_c + v_c \cdot \chi \cdot v_c. \quad (17)$$

The full self-energy is  $\Sigma = \Sigma_x + \Sigma_c$ , where the exchange contribution is given by

$$\Sigma_x = - \sum_i^{\text{occ}} \psi_i(\mathbf{r}) v_c(\mathbf{r}, \mathbf{r}') \psi_i^*(\mathbf{r}'). \quad (18)$$

$V_{xc}$  is the exchange-correlation potential entering the KS Hamiltonian.

We compared QP energies obtained by performing three types of calculations, which we denote as (i)  $G^{\text{SC}}W^{\text{SC}}$ , (ii)  $G^{\text{SC}}W^{\text{VE}}$ , and (iii)  $G^{\text{VE}}W^{\text{VE}}$ , where, as in previous sections, VE and SC denote different core-valence partitions. In i, both the  $G$  and the DM (hence  $W$ ) are computed including semicore electrons, which corresponds to the most complete and accurate representation of the electronic screening. Calculations ii differ from i in the treatment of  $W$ : in ii,  $\tilde{\epsilon}^{\text{VE}}$  instead of  $\tilde{\epsilon}^{\text{SC}}$ , respectively is used; in iii, both  $G$  and  $W$  are computed using only the VE partition. The hybrid calculation, ii, is presented for analysis purposes, to identify the contribution of the semicore electrons to the screened Coulomb potential.

In Table II we report the computed ionization energies, electron affinities, and gaps for calculations i, ii, and iii along with the LDA KS values, for three classes of diatomic molecules: alkali halides, alkali dimers, and alkaline earth oxides. While there are regularities within each class, there are important differences between classes.

In contrast to previous evidence that the inclusion of semicore states results in reduced band gaps,<sup>46,47</sup> for the molecules considered in our study we found reductions or increases in the band gaps, depending on the system. Alkali halides and alkali dimers exhibit larger band gaps for the  $G^{\text{SC}}W^{\text{SC}}$ -type calculation compared to their VE counterpart ( $G^{\text{VE}}W^{\text{VE}}$ ), however, alkaline earth oxides show the opposite trend. Gomez-Abal *et al.*<sup>7</sup> also observed similar findings for

TABLE II. Energies of the highest occupied (HOMO) and lowest unoccupied (LUMO) energy levels (in eV) of several diatomic molecules, obtained using density functional theory calculations within the LDA ( $E^{\text{SC}}$ ,  $E^{\text{VE}}$ ) using two core-valence partitions, semicore (SC) and valence only (VE), within non-self-consistent  $GW$  calculations. The experimental ionization potential and electron affinity are given for the corresponding HOMO and LUMO levels.

		HOMO	LUMO	Gap
NaCl	$E^{\text{SC}}$	-5.36	-1.99	3.37
	$E^{\text{VE}}$	-5.3	-1.71	3.59
	$G^{\text{SC}}W^{\text{SC}}$	-9.19	-0.29	8.9
	$G^{\text{SC}}W^{\text{VE}}$	-9.19	-0.27	8.92
	$G^{\text{VE}}W^{\text{VE}}$	-9.18	-0.53	8.65
	Expt.	9.2 <sup>33</sup>	0.769 <sup>34</sup>	8.43
KCl	$E^{\text{SC}}$	-4.97	-1.55	3.42
	$E^{\text{VE}}$	-4.88	-1.24	3.64
	$G^{\text{SC}}W^{\text{SC}}$	-8.68	-0.06	8.62
	$G^{\text{SC}}W^{\text{VE}}$	-8.69	0.025	8.72
	$G^{\text{VE}}W^{\text{VE}}$	-8.68	-0.32	8.36
	Expt.	8.3 <sup>35</sup>	0.582 ± 0.01 <sup>36</sup>	7.72
KI	$E^{\text{SC}}$	-4.59	-1.71	2.88
	$E^{\text{VE}}$	-4.53	-1.41	3.12
	$G^{\text{SC}}W^{\text{SC}}$	-7.56	-0.22	7.34
	$G^{\text{SC}}W^{\text{VE}}$	-7.56	-0.14	7.42
	$G^{\text{VE}}W^{\text{VE}}$	-7.56	-0.44	7.12
	Expt.	7.5 ± 0.4 <sup>37</sup>	0.5 ± 0.1 <sup>38</sup>	7.0
Li <sub>2</sub>	$E^{\text{SC}}$	-3.18	-1.76	1.42
	$E^{\text{VE}}$	-3.17	-1.73	1.44
	$G^{\text{SC}}W^{\text{SC}}$	-4.91	-0.71	4.2
	$G^{\text{SC}}W^{\text{VE}}$	-4.95	-0.71	4.24
	$G^{\text{VE}}W^{\text{VE}}$	-4.94	-0.74	4.20
	Expt.	5.112 ± 0.0003 <sup>39</sup>		
Na <sub>2</sub>	$E^{\text{SC}}$	-3.14	-1.79	1.35
	$E^{\text{VE}}$	-3.16	-1.8	1.36
	$G^{\text{SC}}W^{\text{SC}}$	-5.19	-0.78	4.41
	$G^{\text{SC}}W^{\text{VE}}$	-5.21	-0.79	4.42
	$G^{\text{VE}}W^{\text{VE}}$	-4.96	-0.69	4.27
	Expt.	4.8951 ± 0.0002 <sup>40</sup>	0.43 ± 0.015 <sup>41</sup>	4.47
K <sub>2</sub>	$E^{\text{SC}}$	-2.54	-1.58	0.96
	$E^{\text{VE}}$	-2.6	-1.65	0.95
	$G^{\text{SC}}W^{\text{SC}}$	-4.22	-0.60	3.62
	$G^{\text{SC}}W^{\text{VE}}$	-4.03	-0.52	3.51
	$G^{\text{VE}}W^{\text{VE}}$	-4.18	-0.78	3.4
	Expt.	4.0637 ± 0.0002 <sup>40</sup>	0.497 ± 0.012 <sup>42</sup>	3.57
Rb <sub>2</sub>	$E^{\text{SC}}$	-2.43	-1.52	0.91
	$E^{\text{VE}}$	-2.52	-1.6	0.92
	$G^{\text{SC}}W^{\text{SC}}$	-3.88	-0.51	3.37
	$G^{\text{SC}}W^{\text{VE}}$	-3.88	-0.62	3.26
	$G^{\text{VE}}W^{\text{VE}}$	-3.9	-0.74	3.17
	Expt.	3.9 ± 0.1 <sup>41</sup>	0.498 ± 0.015 <sup>43</sup>	3.402
CaO	$E^{\text{SC}}$	-3.904	-2.33	1.574
	$E^{\text{VE}}$	-4.04	-1.92	2.06
	$G^{\text{SC}}W^{\text{SC}}$	-6.46	-0.55	5.91
	$G^{\text{SC}}W^{\text{VE}}$	-6.41	-0.51	5.9
	$G^{\text{VE}}W^{\text{VE}}$	-6.88	-0.55	6.33
	Expt.	6.66 ± 0.18 <sup>44</sup>		
SrO	$E^{\text{SC}}$	-3.67	-2.21	1.46
	$E^{\text{VE}}$	-3.86	-1.97	1.89
	$G^{\text{SC}}W^{\text{SC}}$	-6.01	-0.39	5.62
	$G^{\text{SC}}W^{\text{VE}}$	-5.99	-0.36	5.63
	$G^{\text{VE}}W^{\text{VE}}$	-6.45	-0.52	5.93
	Expt.	6.6 ± 0.18 <sup>44</sup>		

solids, e.g., GaAs and CaSe gaps obtained with PPs were smaller than their all-electron counterparts.

For several semiconductors and insulators, it was found that non-self-consistent  $GW$  PP calculations with VE partitions were successful in reproducing band gaps of most semiconductors and insulators and that often all-electron non-self-consistent  $GW$  results were worse than the corresponding PP  $GW$  ones,<sup>7</sup> compared to experiments. This is possibly due to compensating approximations in the  $GW$  PP formulation such as core-valence partitioning and use of pseudo-wave functions.<sup>16</sup> Our results for molecules confirm this finding for gaps for two classes of systems (alkali halides and alkaline earth oxides), but for alkali dimers the SC results are in better agreement with experiments than the VE results. Below we summarize our findings for each class of molecules considered here.

### A. Alkali halide molecules

The HOMO energy level from  $GW$  calculations compares well with the measured ionization potential. The agreement of the LUMO energy with the electron affinity and of the computed QP gap with the measured one is worse (the gap is larger) for the SC calculation. For example, for KI and KCl the difference between computed and measured QP gaps is 5% and 11%, respectively, for SC, compared to 2% and 8% for VE calculations. By isolating the effect of core polarization we observed that the difference in the computed QP band gaps is of the order of 0.1 eV. The agreement with the experiment worsens for the “hybrid” calculations compared to the SC calculation, by 1% and 2% for KI and KCl, respectively.

### B. Alkaline earth oxides

Similarly to the case of alkali halides, the HOMO energy is in worse agreement with the measured ionization potential for the SC partition. For SrO, for example, the difference between the HOMO energy and the ionization potential is 9% for the  $G^{\text{SC}}W^{\text{SC}}$  calculation, compared to  $\approx 2\%$  for the  $G^{\text{VE}}W^{\text{VE}}$  calculation. Isolating the core polarization effects hardly affects the difference between the HOMO and the ionization potential (0.3% increase). The core polarization effect is negligible for the band gap in these oxides, consistent with the more moderate SC screening that can be discerned from the DOS [Fig. 2(f)] and the IPR analysis [Fig. 3(c)].

### C. Alkali dimers

The trend noticed above, where SC results are in worse agreement with the experiment compared to VE results, is reversed for alkali dimers, which are covalently bonded, as opposed to the other molecules, where there is (partial) charge transfer between anions and cations. The SC results for QP gaps and LUMO energies are in better agreement with experiment than the VE results are. Taking the K<sub>2</sub> and Rb<sub>2</sub> molecules as examples, the QP gaps are within 1.4% and 1% of the experiment for SC, versus 4.5% and 7% for VE, respectively. Core polarization affects the QP band gap by up to 0.11 eV for K<sub>2</sub> and Rb<sub>2</sub>. The hybrid calculation worsens the agreement with the experiment compared to  $G^{\text{SC}}W^{\text{SC}}$ : 1.6% and 4% for K<sub>2</sub> and Rb<sub>2</sub>. The SC results are in better agreement

TABLE III. Matrix elements of the self-energy (in eV) for the exchange  $\Sigma_x$ , correlation  $\Sigma_c$ , and exchange-correlation potential  $V_{xc}$  for KI, K<sub>2</sub>, and SrO along with the Kohn-Sham energies ( $E^{KS}$ ) and QP energies (in eV) of the highest occupied (HOMO) and lowest unoccupied (LUMO) energy levels and the gap for (i)  $G^{SC}W^{SC}$ , (ii)  $G^{SC}W^{VE}$ , and (iii)  $G^{VE}W^{VE}$  calculations.

		$E^{KS}$	$\langle \Sigma_x \rangle$	$\langle V_{xc} \rangle$	$\langle \Sigma_x \rangle - \langle V_{xc} \rangle$	$\langle \Sigma_c \rangle$	$E^{QP}$
KI							
HOMO	$G^{SC}W^{SC}$	-4.59	-13.56	-10.17	-3.39	0.42	-7.56
	$G^{SC}W^{VE}$	-4.59	-13.56	-10.17	-3.39	0.42	-7.56
	$G^{VE}W^{VE}$	-4.54	-13.51	-10.1	-3.41	0.39	-7.56
LUMO	$G^{SC}W^{SC}$	-1.71	-1.11	-3.43	2.32	-0.83	-0.22
	$G^{SC}W^{VE}$	-1.71	-1.11	-3.43	2.32	-0.75	-0.14
	$G^{VE}W^{VE}$	-1.41	-0.39	-1.71	1.32	-0.35	-0.44
Gap	$G^{SC}W^{SC}$	2.88	12.45	6.74	5.71	-1.25	7.34
	$G^{SC}W^{VE}$	2.88	12.45	6.74	5.71	-1.17	7.42
	$G^{VE}W^{VE}$	3.13	13.12	8.39	4.73	-0.74	7.12
K <sub>2</sub>							
HOMO	$G^{SC}W^{SC}$	-2.54	-5.38	-4.65	-0.73	-0.95	-4.22
	$G^{SC}W^{VE}$	-2.54	-5.38	-4.65	-0.73	-0.76	-4.03
	$G^{VE}W^{VE}$	-2.6	-4.69	-3.56	-1.13	-0.45	-4.18
LUMO	$G^{SC}W^{SC}$	-1.58	-1.49	-3.76	2.27	-1.29	-0.6
	$G^{SC}W^{VE}$	-1.58	-1.49	-3.76	2.27	-1.21	-0.52
	$G^{VE}W^{VE}$	-1.65	-0.91	-2.77	1.86	-0.99	-0.78
Gap	$G^{SC}W^{SC}$	0.96	3.89	0.89	3.0	-0.34	3.62
	$G^{SC}W^{VE}$	0.96	3.89	0.89	3.0	-0.45	3.51
	$G^{VE}W^{VE}$	0.95	3.78	0.79	2.99	-0.54	3.4
SrO							
HOMO	$G^{SC}W^{SC}$	-3.67	-21.53	-17.01	-4.52	2.18	-6.01
	$G^{SC}W^{VE}$	-3.67	-21.53	-17.01	-4.52	2.21	-5.98
	$G^{VE}W^{VE}$	-3.87	-20.69	-15.75	-4.94	2.36	-6.45
LUMO	$G^{SC}W^{SC}$	-2.21	-1.89	-4.68	2.79	-0.97	-0.39
	$G^{SC}W^{VE}$	-2.21	-1.89	-4.68	2.79	-0.93	-0.35
	$G^{VE}W^{VE}$	-1.97	-1.08	-3.13	2.05	-0.6	-0.52
Gap	$G^{SC}W^{SC}$	1.46	19.64	12.33	7.31	-3.15	5.62
	$G^{SC}W^{VE}$	1.46	19.64	12.33	7.31	-3.14	5.63
	$G^{VE}W^{VE}$	1.9	19.61	12.62	6.99	-2.96	5.93

than the VE results with the experimental gaps for all the alkali dimers, unlike for the alkali halide molecules.

Overall we find that if accuracies of the order of 100–200 meV in calculated QP eigenvalues are desired, the inclusion of semicore states is necessary not only in the calculation of wave functions and thus of  $\Sigma_x$  and  $V_{xc}$ , but also in the evaluation of  $\Sigma_c$ . We thus confirm previous work indicating that the inclusion of even fairly strongly bound semicore states that might be thought to be inert, based on a large denominator in Eq. (4), can substantially contribute to HOMO and LUMO QP energies. For example, in the case of Rb<sub>2</sub> (containing the alkali atom with the largest polarizability), the contribution of semicore polarization to the LUMO state and the gap is about 100 meV. For K<sub>2</sub>, the contributions to the HOMO, LUMO, and gap are about 200, 80, and 110 meV, respectively. For alkali halides such as KCl and KI, the contribution of semicore polarization to the computed gap and LUMO energy is of the order of 100 meV. However, if errors of the orders of 100–200 meV may be tolerated, e.g., in analyzing trends of QP gaps within certain classes of systems, one may use an approximate dielectric screening computed with the VE partition, with substantial computational savings.

## VII. SUMMARY

We have presented a new approach for calculating and analyzing the effect of electronic semicore polarization on dielectric, vibrational, and electronic excitation properties of molecules and solids, based on the spectral decomposition of the dielectric matrix. Including semicore electrons leads to additional eigenmodes in the DBS with eigenvalues substantially different from unity. Even if the eigenmodes are localized, as often happens, they contribute to screening. Polarization arising from semicore electrons may contribute  $\sim 10\%$  to both the dielectric constants and the transverse optical phonon modes, with effects being greater for systems constituting the larger and therefore more polarizable atoms. The distribution of dielectric eigenvalues and the IPR analysis for molecules show that there is no clear distinction between eigenmodes due to semicore response versus those from valence electrons; there is a continuum, with the mixing being more widespread for molecules with larger atoms. The effects of the core polarization, e.g., on computed QP gaps, are found to be different for molecules with covalent and ionic bonds. The GW predictions of QP energies and of the gap have been quantified and trends within classes of diatomic molecules have been identified. If a precision of  $\sim 200$  meV in these

energies is needed, semicore electrons must be included in the calculations. Otherwise they may be discarded, with substantial savings in the calculations.

### ACKNOWLEDGMENTS

We thank Y. Ping, Y. Li, H.-V. Nguyen, and D. Rocca for useful discussions. This work was supported by DOE/SciDAC-e Grant No. DE-FC02-06ER25777, DOE/SciDac Grant No. DE-FC02-06ER25794, and DOE/BES Grant No. DE-FG02-06ER46262 (G.G. and T.A.P.). We used the Extreme Science and Engineering Discovery Environment (XSEDE), which is supported by National Science Foundation Grant No. OCI-1053575, and the NERSC facility at LBNL. Research was carried out in part at the Center for Functional Nanomaterials, Brookhaven National Laboratory, which is supported by the US Department of Energy, Office of Basic Energy Sciences, under Contract No. DE-AC02-98CH10886D. A. Kaur was supported by the Guru Gobind Singh Fellowship. W.E.P. acknowledges support from the Simons Foundation and the hospitality of the Graphene Research Center, National University of Singapore, during the latter stage of this work.

### APPENDIX: QUASIPARTICLE ENERGIES

We provide the matrix elements of the self-energy (exchange,  $\Sigma_x$ ; and correlation,  $\Sigma_c$  terms), exchange correlation potential  $V_{xc}$ , LDA KS energies, and computed QP energies for the HOMO, LUMO, and gap of a representative molecule from each class of molecules considered in this study. The results are shown for three types of calculations as described in Sec. VI: (i)  $G^{\text{SC}}W^{\text{SC}}$ , (ii)  $G^{\text{SC}}W^{\text{VE}}$ , and (iii)  $G^{\text{VE}}W^{\text{VE}}$ .

### 1. Comparison with the literature

For the  $sp$ -bonded solids considered in Refs. 7 and 16, the authors found that even though there is a large difference in the PP (VE) and all-electron matrix elements of  $\Sigma_x$  and  $V_{xc}$ , the sum ( $\Sigma_x - V_{xc}$ ) is similar in the two cases. The way the latter sum is computed gave negligible differences in the computed  $E_{\text{gap}}$ , with major differences coming instead from the  $\Sigma_c$  matrix elements. However, while for the  $sp$ -bonded molecules (alkali dimers), we found a trend similar to that in Refs. 7 and 16, this trend did not hold for alkali halides and alkaline earth oxides (Table III).

For example, for  $\text{K}_2$ , the difference in ( $\langle \Sigma_x \rangle - \langle V_{xc} \rangle$ ) obtained with VE versus SC partitions is negligible. The remaining difference between the VE and the SC band gaps comes from the underestimation of  $\Sigma_c$  in the VE calculations ( $\approx 0.2$  eV). Instead, in the case of alkali halides, such as KI, the difference in the gap between the VE and the SC calculations arises from the difference in the matrix elements of both  $\Sigma_x$  and  $V_{xc}$  (of the order of 0.7 and 1.7 eV, respectively). The cancellation is incomplete and it contributes to the difference between the SC and the VE band gaps, together with the difference in the matrix elements of  $\Sigma_c$ . There is an overestimation in the correlation energy in VE calculations ( $\approx 0.5$  eV), which tends to reduce the effect of incomplete cancellation between the matrix elements of  $\Sigma_x$  and  $V_{xc}$ . Similarly, in the case of alkaline earth oxides such as SrO, the cancellation is incomplete ( $\langle \Sigma_x \rangle - \langle V_{xc} \rangle \approx 0.3$  eV), which, along with the overestimation of the KS band gap ( $\approx 0.4$  eV) in VE-only calculations and the difference in the correlation term ( $\approx 0.2$  eV), leads to a difference between the SC and the VE computed band gaps.

\*Corresponding author: ackaur@ucdavis.edu

<sup>1</sup>A. Baldereschi and E. Tosatti, *Solid State Commun.* **29**, 131 (1979).  
<sup>2</sup>R. Car, E. Tosatti, S. Baroni, and S. Leelaprute, *Phys. Rev. B* **24**, 985 (1981).  
<sup>3</sup>M. S. Hybertsen and S. G. Louie, *Phys. Rev. B* **35**, 5585 (1987).  
<sup>4</sup>P. B. Allen, M. L. Cohen, and D. R. Penn, *Phys. Rev. B* **38**, 2513 (1988).  
<sup>5</sup>E. L. Shirley, X. Zhu, and S. G. Louie, *Phys. Rev. Lett.* **69**, 2955 (1992).  
<sup>6</sup>E. L. Shirley, X. Zhu, and S. G. Louie, *Phys. Rev. B* **56**, 6648 (1997).  
<sup>7</sup>R. Gómez-Abal, X. Li, M. Scheffler, and C. Ambrosch-Draxl, *Phys. Rev. Lett.* **101**, 106404 (2008).  
<sup>8</sup>A. Marini, G. Onida, and R. Del Sole, *Phys. Rev. Lett.* **88**, 016403 (2001).  
<sup>9</sup>M. S. Hybertsen and S. G. Louie, *Phys. Rev. Lett.* **55**, 1418 (1985).  
<sup>10</sup>M. S. Hybertsen and S. G. Louie, *Phys. Rev. B* **34**, 5390 (1986).  
<sup>11</sup>M. Rohlfiing, P. Krüger, and J. Pollmann, *Phys. Rev. Lett.* **75**, 3489 (1995).  
<sup>12</sup>M. Rohlfiing, P. Krüger, and J. Pollmann, *Phys. Rev. B* **57**, 6485 (1998).  
<sup>13</sup>M. Rohlfiing, P. Krüger, and J. Pollmann, *Phys. Rev. B* **56**, R7065 (1997).

<sup>14</sup>W. Ku and A. G. Eguiluz, *Phys. Rev. Lett.* **89**, 126401 (2002).  
<sup>15</sup>L. Hedin, *Phys. Rev.* **139**, A796 (1965).  
<sup>16</sup>X.-Z. Li, R. Gómez-Abal, H. Jiang, C. Ambrosch-Draxl, and M. Scheffler, *New J. Phys.* **14**, 023006 (2012).  
<sup>17</sup>P. Umari and S. Fabris, *J. Chem. Phys.* **136**, 174310 (2012).  
<sup>18</sup>H. F. Wilson, F. Gygi, and G. Galli, *Phys. Rev. B* **78**, 113303 (2008).  
<sup>19</sup>H. F. Wilson, D. Lu, F. Gygi, and G. Galli, *Phys. Rev. B* **79**, 245106 (2009).  
<sup>20</sup>J. A. Van Vechten and R. M. Martin, *Phys. Rev. Lett.* **28**, 446 (1972).  
<sup>21</sup>S. G. Louie, J. R. Chelikowsky, and M. L. Cohen, *Phys. Rev. Lett.* **34**, 155 (1975).  
<sup>22</sup>H.-V. Nguyen and S. de Gironcoli, *Phys. Rev. B* **79**, 205114 (2009).  
<sup>23</sup>H.-V. Nguyen and S. de Gironcoli, *Phys. Rev. B* **79**, 115105 (2009).  
<sup>24</sup>P. Giannozzi, S. Baroni, N. Bonini, M. Calandra, R. Car, C. Cavazzoni, D. Ceresoli, G. L. Chiarotti, M. Cococcioni, I. Dabo *et al.*, *J. Phys.: Condens. Matter* **21**, 395502 (2009).  
<sup>25</sup>C. Hartwigsen, S. Goedecker, and J. Hutter, *Phys. Rev. B* **58**, 3641 (1998).  
<sup>26</sup>D. Porezag, M. R. Pederson, and A. Y. Liu, *Phys. Rev. B* **60**, 14132 (1999).  
<sup>27</sup>S. G. Louie, S. Froyen, and M. L. Cohen, *Phys. Rev. B* **26**, 1738 (1982).  
<sup>28</sup>W. Yu, C. Jin, and A. Kohlmeyer, *J. Phys.: Condens. Matter* **19**, 086209 (2007).

- <sup>29</sup>V. I. Zinenko and A. S. Fedorov, *Sov. Phys. Solid State* **36**, 742 (1994).
- <sup>30</sup>J. Zhang, L. Zhang, T. Cui, Y. Li, Z. He, Y. Ma, and G. Zou, *Phys. Rev. B* **75**, 104115 (2007).
- <sup>31</sup>G. Roma, C. M. Bertoni, and S. Baroni, *Solid State Commun.* **98**, 203 (1996).
- <sup>32</sup>J. Y. Zhang, L. J. Zhang, T. Cui, Y. L. Niu, Y. M. Ma, Z. He, and G. T. Zou, *J. Phys.: Condens. Matter* **19**, 425218 (2007).
- <sup>33</sup>D. J. Williams, *Aust. J. Chem.* **35**, 1531 (1982).
- <sup>34</sup>C. De Vreugd, R. Wijnaendts Van Resandt, J. Los, B. Smith, and R. L. Champion, *Chem. Phys.* **42**, 305 (1979).
- <sup>35</sup>H. Bloom and D. J. Williams, *J. Chem. Phys.* **75**, 4636 (1981).
- <sup>36</sup>T. M. Miller, D. G. Leopold, K. K. Murray, and W. C. Lineberger, *J. Chem. Phys.* **85**, 2368 (1986).
- <sup>37</sup>H.-H. Emons, W. Horlbeck, and D. Kiessling, *Z. Anorg. Allg. Chem.* **488**, 212 (1982).
- <sup>38</sup>Y. A. Yang, L. A. Bloomfield, C. Jin, L. Wang, and R. E. Smalley, *J. Chem. Phys.* **96**, 2453 (1992).
- <sup>39</sup>M. W. McGeoch and R. E. Schlier, *Chem. Phys. Lett.* **99**, 347 (1983).
- <sup>40</sup>M. M. Kappes, P. Radi, M. Schar, and E. Schumacher, *Chem. Phys. Lett.* **113**, 243 (1985).
- <sup>41</sup>K. M. McHugh, J. G. Eaton, G. H. Lee, H. W. Sarkas, L. H. Kidder, J. T. Snodgrass, M. R. Manaa, and K. H. Bowen, *J. Chem. Phys.* **91**, 3792 (1989).
- <sup>42</sup>J. G. Eaton, H. W. Sarkas, S. T. Arnold, K. M. McHugh, and K. H. Bowen, *Chem. Phys. Lett.* **193**, 141 (1992).
- <sup>43</sup>M. M. Kappes and E. Schumacher, *Surface Sci.* **156**, 1 (1985).
- <sup>44</sup>N. F. Dalleska and P. B. Armentrout, *Int. J. Mass Spectrom. Ion Process.* **134**, 203 (1994).
- <sup>45</sup>H.-V. Nguyen, T. A. Pham, D. Rocca, and G. Galli, *Phys. Rev. B* **85**, 081101(R) (2012).
- <sup>46</sup>M. L. Tiago, S. Ismail-Beigi, and S. G. Louie, *Phys. Rev. B* **69**, 125212 (2004).
- <sup>47</sup>M. van Schilfgaarde, T. Kotani, and S. V. Faleev, *Phys. Rev. B* **74**, 245125 (2006).